European Journal of Inorganic Chemistry

EurJIC
European Journal of Inorganic Chemistry

Chemistry Europe
European Chemical Societies Publishing

RESEARCH ARTICLE OPEN ACCESS

Fluorescent Zinc(II) Complexes with a *N*,*N*,*N*-Tridentate Ligand Based on the Bis(imidazo[1,5-*a*]pyridine)methane Scaffold

Chiara Vola[1] | Gioele Colombo[1] | Anita Cinco[1,2] | Bruno Therrien[3] | G. Attilio Ardizzoia[1] | Stefano Brenna[1]

[1]Department of Science and High Technology, University of Insubria and CIRCC, Como, Italy | [2]University School for Advanced Studies IUSS, Pavia, Italy | [3]Institute of Chemistry, University of Neuchatel, Neuchatel, Switzerland

Correspondence: Gioele Colombo (gioele.colombo@uninsubria.it) | Stefano Brenna (stefano.brenna@uninsubria.it)

Received: 29 April 2026 | **Revised:** 7 July 2026 | **Accepted:** 9 July 2026

Keywords: blue emission | density functional theory | fluorescence | *N*-ligands | zinc(II) complexes

ABSTRACT

A *N*,*N*,*N*-tridentate ligand (3,3′-(2-(pyridin-2-yl)ethane-1,1-diyl)bis(1-methylimidazo[1,5-*a*]pyridine), $\mathbf{L}^{\mathbf{CH2Py}}$) based on the bis(imidazo[1,5-*a*]pyridine)methane scaffold has been prepared through the introduction of a methylpyridine pendant arm. This functionalization provides an additional donor site, enabling a different coordination mode compared to previously reported bidentate systems. The reaction of this ligand with zinc(II) salts led to the formation of mononuclear complexes ([Zn($\mathbf{L}^{\mathbf{CH2Py}}$)$X_2$], X = Cl, Br, I; [Zn($\mathbf{L}^{\mathbf{CH2Py}}$)Br]($BF_4$); [Zn($\mathbf{L}^{\mathbf{CH2Py}}$)$_2$]($ClO_4$)$_2$), which were fully characterized both in solution (NMR) and in solid state (X-ray). The tridentate coordination mode generates a rigid and stereochemically defined coordination sphere around the zinc center, resulting in the formation of chiral complexes, as supported by NMR analysis. The photophysical properties of ligand and complexes were investigated, revealing that all the derivatives exhibit intense blue fluorescence (λ_{em} = 453 nm for ligand, 419–437 nm for complexes), comparable to that observed for the parent system with unfunctionalized bis(imidazo[1,5-*a*]pyridine)methane (λ_{em} = 450 nm). These results demonstrate that the extension from *N*,*N*- to *N*,*N*,*N*-coordination enhances the structural rigidity and stereochemical complexity of the system while preserving the favorable emissive properties. This work further expands the scope of bis(imidazo[1,5-*a*]pyridine)-based ligands in coordination chemistry and highlights their potential as building blocks for the development of chiral luminescent materials.

1 | Introduction

Multidentate ligands play a pivotal role in coordination chemistry due to their ability to stabilize metal centers and finely tune the structural and electronic properties of the resulting complexes. Their versatility has led to widespread applications across different research areas, including the construction of polynuclear architectures [1], catalysis [2], and the development of functional materials with tailored optical properties [3]. In particular, the rational design of ligand frameworks with multiple donor atoms enables precise control over metal coordination environments, thus directly influencing reactivity and photophysical behavior.

Within this context, tridentate ligands have attracted considerable attention, as they provide an optimal balance between structural rigidity, stability, and coordination flexibility. Among them, *N*,*N*,*N*-donor systems represent a prominent subclass, extensively investigated for their rich coordination chemistry and ability to support a wide range of metal ions [4, 5]. These ligands often enforce well-defined geometries and can promote the formation of discrete mononuclear as well as more complex architectures, while also offering opportunities to modulate electronic properties through ligand functionalization.

Zinc(II) complexes coordinated by *N*,*N*,*N*-tridentate ligands have emerged as particularly appealing systems in the field of

luminescent materials. Owing to the d^{10} electronic configuration of zinc(II), which prevents quenching via *d*–*d* transitions, the emission properties are typically ligand-centered and can be efficiently tuned through structural modifications [6]. As a result, a variety of zinc(II) complexes displaying intense fluorescence have been reported, highlighting their potential for applications in sensing and optoelectronics [7].

Among nitrogen-containing heterocycles, imidazo[1,5-*a*]pyridines have drawn valuable attention, thanks to their noteworthy photophysical properties [8–12] and their synthetic accessibility [13–16]. Both mono- [17–23] and bis-(imidazo[1,5-*a*]pyridines) [24–26] have been widely employed in the synthesis of luminescent coordination compounds, whereas the fluorescent behavior of bis(imidazo[1,5-*a*]pyridine)methane species [27–33], featuring a methylene linker between the two heterocyclic units, has remained comparatively underexplored. In our recent work [34], we investigated bis(imidazo[1,5-*a*]pyridine)methane ligands acting as *N*,*N*-bidentate donors, demonstrating their ability to form fluorescent zinc(II) complexes with attractive blue emission. Building on these findings and aiming to further expand the coordination versatility of this class of ligands, herein we report the functionalization of the bis(imidazo[1,5-*a*]pyridine)methane scaffold with a methylpyridine pendant arm, thus introducing an additional donor site and generating a *N*,*N*,*N*-tridentate ligand. The coordination behavior toward zinc(II) has been investigated by operating either under 1:1 or 1:2 metal:ligand proportions, and particular attention has been devoted to the structural and photophysical properties of the resulting blue-emissive complexes.

2 | Results and Discussion

2.1 | Syntheses of Ligands and Complexes

The bis(imidazo[1,5-*a*]pyridine)methane $\mathbf{L^H}$ was synthesized as previously reported [34]. Subsequent functionalization on the methylene bridge involves the deprotonation with methyl magnesium bromide in diisopropyl ether, followed by reaction with 2-chloromethylpyridine, leading to the formation of the desired functionalized product $\mathbf{L^{CH2Py}}$ in 56% yield (Scheme 1).

Ligand $\mathbf{L^{CH2Py}}$ was then used to prepare different zinc(II) complexes by reaction either with one equivalent of zinc(II) halides to give $[Zn(\mathbf{L^{CH2Py}})X_2]$ (X = Cl, Br, I) or half equivalent of zinc(II) perchlorate hexahydrate, leading to $[Zn(\mathbf{L^{CH2Py}})_2](ClO_4)_2$ (Scheme 1). Additionally, the $[Zn(\mathbf{L^{CH2Py}})Br_2]$ complex was treated with one equivalent of $AgBF_4$, in acetonitrile at room temperature, affording complex $[Zn(\mathbf{L^{CH2Py}})Br]BF_4$ in 85% yield (Scheme 1).

The IR (ATR) spectrum of $\mathbf{L^{CH2Py}}$ (Figure S1) displays absorptions at 1631, 1595, 1570, and 1479 cm^{-1}, attributed to coupled skeletal stretching vibrations (i.e., ring breathing) of the heteroaromatic rings. Compared to the precursor bis(imidazo[1,5-*a*]pyridine)methane species [34], which exhibits absorptions at 1631, 1550, 1518, and 1479 cm^{-1}, as expected, the introduction of the pyridyl pendant arm modifies the vibrational pattern in this region, owing to the contribution of additional pyridyl ring modes. Upon coordination to zinc(II) (Figures S2–S6), the band

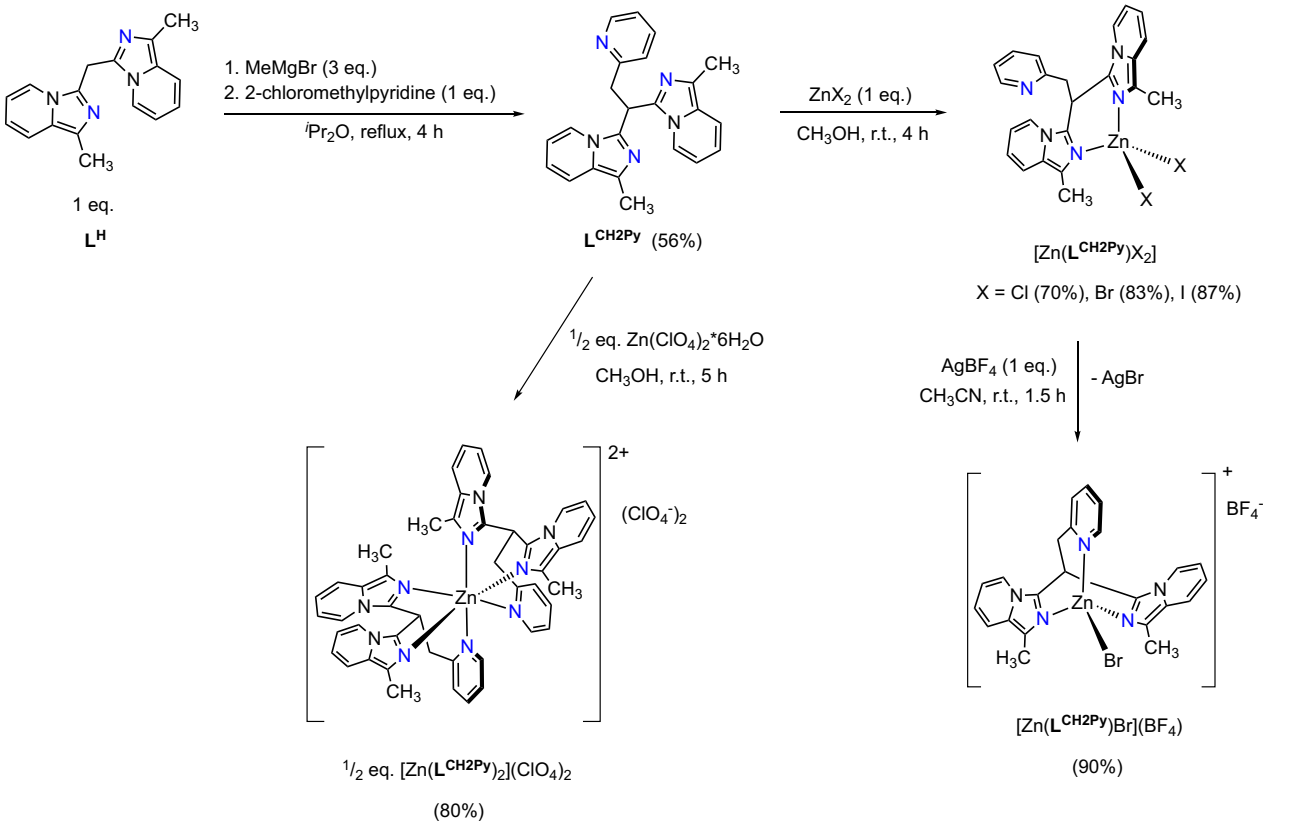

SCHEME 1 | Functionalization of ligand $\mathbf{L^H}$ to give $\mathbf{L^{CH2Py}}$ and syntheses of $[Zn(\mathbf{L^{CH2Py}})X_2]$, $[Zn(\mathbf{L^{CH2Py}})Br](BF_4)$, and $[Zn(\mathbf{L^{CH2Py}})_2](ClO_4)_2$ complexes.

at 1631 cm^{-1} undergoes a shift to 1645 cm^{-1}, while the absorptions at 1595, 1570, and 1479 cm^{-1} remain essentially unchanged. These observations suggest that coordination mainly perturbs the electronic distribution within the imidazo[1,5-*a*]pyridine core, whereas the vibrational modes associated with the pendant pyridyl group are only marginally affected. Moreover, the infrared spectra of complexes $Zn(\mathbf{L}^{\mathbf{CH2Py}})_2](ClO_4)_2$ and $[Zn(\mathbf{L}^{\mathbf{CH2Py}})Br]BF_4$ showed the presence of uncoordinated perchlorate (broad band at 1082 cm^{-1}) and uncoordinated tetrafluoroborate (broad band in the range 1036–991 cm^{-1}). Worth noting, the IR spectra (Figures S2–S6) do not display stretchings in the 3400–3600 cm^{-1} region associated with O—H groups, indicating the absence of water in the bulk material.

2.2 | NMR Investigation

In the ^1H NMR (CD_2Cl_2, 25 °C) spectrum of $\mathbf{L}^{\mathbf{CH2Py}}$ (Figure S7), the signals attributable to the imidazo[1,5-*a*]pyridine nucleus are clearly observed in the 6.30–8.50 ppm range (aromatic protons) and at 2.43 ppm (CH_3). The spectrum also displays the expected signals associated with the aliphatic bridge: a triplet at 5.56 ppm (C*H*, $^3J = 7.5$ Hz) and a doublet at 3.95 ppm (CH_2, $^2J = 7.5$ Hz). The corresponding signals in the $^{13}C\{^1H\}$ NMR spectrum further confirm the successful synthesis of the ligand (Figure S8): resonances are found at 39.1 ppm (*C*H_2) and 38.0 ppm (*C*H). Overall, coordination with the zinc center induces slight variations in the ^1H NMR chemical shifts. For $[Zn(\mathbf{L}^{\mathbf{CH2Py}})Cl_2]$, the signals associated with the aliphatic bridge are found at 5.76 ppm (C*H*, $^3J = 7.5$ Hz) and at 3.56 ppm (CH_2, $^2J = 7.5$ Hz), whereas the methyl group in position 1 of the imidazo[1,5-*a*]pyridine framework shifts downfield from 2.43 ppm (in $\mathbf{L}^{\mathbf{CH2Py}}$) to 2.75 ppm in the complex (Figure S9). In the $^{13}C\{^1H\}$ NMR spectrum, both the aliphatic bridge resonances are shifted, appearing at 33.4 ppm (38.0 in $\mathbf{L}^{\mathbf{CH2Py}}$) and at 44.9 ppm (39.1 in $\mathbf{L}^{\mathbf{CH2Py}}$). Similarly, the methyl group in position 1 of the imidazo[1,5-*a*] pyridine framework shifts upfield from 12.8 ppm ($\mathbf{L}^{\mathbf{CH2Py}}$) to 12.2 ppm in the complex (Figure S10). A very similar pattern is also observed in the spectra of the analogous $[Zn(\mathbf{L}^{\mathbf{CH2Py}})Br_2]$ and $[Zn(\mathbf{L}^{\mathbf{CH2Py}})I_2]$ complexes (Figures S11–S14), with the only exception of the methyl group in position 1 of the imidazo[1,5-*a*]pyridine framework, which appears to be slightly shifted at 2.79 ppm for $[Zn(\mathbf{L}^{\mathbf{CH2Py}})Br_2]$ and 2.86 ppm for $[Zn(\mathbf{L}^{\mathbf{CH2Py}})I_2]$. In the corresponding $^{13}C\{^1H\}$ NMR spectra, these signals are shifted to 12.6 ppm for $[Zn(\mathbf{L}^{\mathbf{CH2Py}})Br_2]$ and 13.2 ppm for $[Zn(\mathbf{L}^{\mathbf{CH2Py}})I_2]$. The pattern of the aliphatic protons remains very similar in both free ligand and the $[Zn(\mathbf{L}^{\mathbf{CH2Py}})X_2]$ complexes. This suggests that ligand $\mathbf{L}^{\mathbf{CH2Py}}$ is coordinated in a *N*,*N*-bidentate mode to zinc(II) halides, with the methylpyridine pendant arm not coordinated to the metal, eventually leading to the formation of tetrahedral complexes. Conversely, when the $[Zn(\mathbf{L}^{\mathbf{CH2Py}})Br_2]$ is reacted with $AgBF_4$, this induces the replacement of one bromide ligand and forces the methylpyridine pendant arm to coordinate to the zinc(II) center. The ^1H and the $^{13}C\{^1H\}$ NMR spectra (CD_3CN, 25 °C) of $[Zn(\mathbf{L}^{\mathbf{CH2Py}})Br]BF_4$ are reported in the Supporting Information (Figures S15 and S16). Worthy of note, the two methyl groups in position 1 of each imidazo[1,5-*a*]pyridine skeleton generate one single signal resonating at 2.65 ppm, whereas the methinic and methylenic protons of the bridge are respectively found as triplet at 5.85 ppm ($^3J = 5.3$ Hz) and doublet at 3.73 ppm ($^3J = 5.3$ Hz). All these features are indicative of a symmetric structure for the complex $[Zn(\mathbf{L}^{\mathbf{CH2Py}})Br]BF_4$.

On the other hand, the ^1H NMR spectrum (CD_2Cl_2, 25 °C) of $[Zn(\mathbf{L}^{\mathbf{CH2Py}})_2](ClO_4)_2$ appears markedly different, showing a splitting of the aromatic protons in the range 9.20–6.20 ppm, as well as two resonances centered at 4.10 and 3.89 ppm attributable to diastereotopic methylene protons of the pyridyl pendant arm (Figure S17). More importantly, the methyl groups of the imidazo[1,5-*a*]pyridine moieties on the same bis(imidazo[1,5-*a*]pyridine)methane ligand appear as two separate singlets respectively at 2.29 and 1.68 ppm (^1H NMR) and 11.1 and 12.4 ppm ($^{13}C\{^1H\}$ NMR) (Figure S18). This indicates a lack of symmetry and the presence of two non-equivalent nitrogen atoms coordinated to the zinc(II) center, leading to a mixture of enantiomers in solution. As proof, ^1H NMR spectra of $[Zn(\mathbf{L}^{\mathbf{CH2Py}})_2](ClO_4)_2$ were acquired in the presence of 1 and 2 equivalents of tetrabutylammonium Δ-tris(tetrachloro-1, 2-benzenediolato)phosphate(V) (Δ-TRISPHAT) [35]. As expected, upon addition of Δ-TRISPHAT, a pair of diastereoisomers was generated, as evidenced by the splitting of the two signals attributed to the methyl groups in position 1 of the two imidazopyridines (Figure 1). All these features have been subsequently corroborated by X-ray single-crystal diffraction analysis and density functional theory (DFT) investigation (vide infra).

2.3 | X-Ray Characterization

The single crystal X-ray structure analyses of ligand $\mathbf{L}^{\mathbf{CH2Py}}$, complexes $[Zn(\mathbf{L}^{\mathbf{CH2Py}})Br_2]\cdot H_2O$ and $[Zn(\mathbf{L}^{\mathbf{CH2Py}})_2(OH_2)](ClO_4)_2$ are presented in Figures 2–4 respectively. Bond lengths and angles (Table S1) are comparable to those reported in the literature for similar systems [34]. Brown block single crystals of $\mathbf{L}^{\mathbf{CH2Py}}$ were obtained by slow (overnight) evaporation of a diethyl ether saturated solution of the ligand. As expected, the *N*-imidazole atoms exhibit an *anti*-conformation (Figure 2), while the methylene bridge imposes an angle of 112.71° between the two imidazo[1,5-*a*]pyridine scaffolds (Figure S19).

Complex $[Zn(\mathbf{L}^{\mathbf{CH2Py}})Br_2]\cdot H_2O$ crystallized as a water solvate by slow diffusion of hexane in a saturated acetone solution, giving yellow prism single crystals. The zinc(II) center has a N_2Br_2 surrounding (Zn1—Br1 = 2.3833(10); Zn1—Br2 = 2.3658(10); Zn1—N2 = 2.024(5); Zn1-N4 = 2.031(5)), in a faintly distorted tetrahedral geometry ($\tau_4 = 0.90$ [36]). The complex crystallized in the presence of one adventitious water molecule, which dictates the orientation of the methyl-pyridinyl pendant arm in the crystal (Figure 3). As emphasized in Figure 3, the N(pyridyl) atom interacts with the water molecule, forming a hydrogen bond (O1···N1 distance = 2.940(1) Å, O1—H···N1 angle = 123.69(10)°). Nevertheless, all these structural findings are fully consistent with the ^1H NMR spectroscopic data. Given the close spectroscopic similarities observed for $[Zn(L^{\mathbf{CH2Py}})Cl_2]$ and $[Zn(L^{\mathbf{CH2Py}})I_2]$, it is reasonable to infer that these halide complexes display analogous structural features in solution and in the solid state.

Complex $[Zn(\mathbf{L}^{\mathbf{CH2Py}})_2(OH_2)](ClO_4)_2$ crystallized with one coordinated water molecule (Zn1—O1 bond length = 2.072(4) Å), most likely retained from the crystallization solvent: indeed, orange plate single crystals of the complex were obtained by

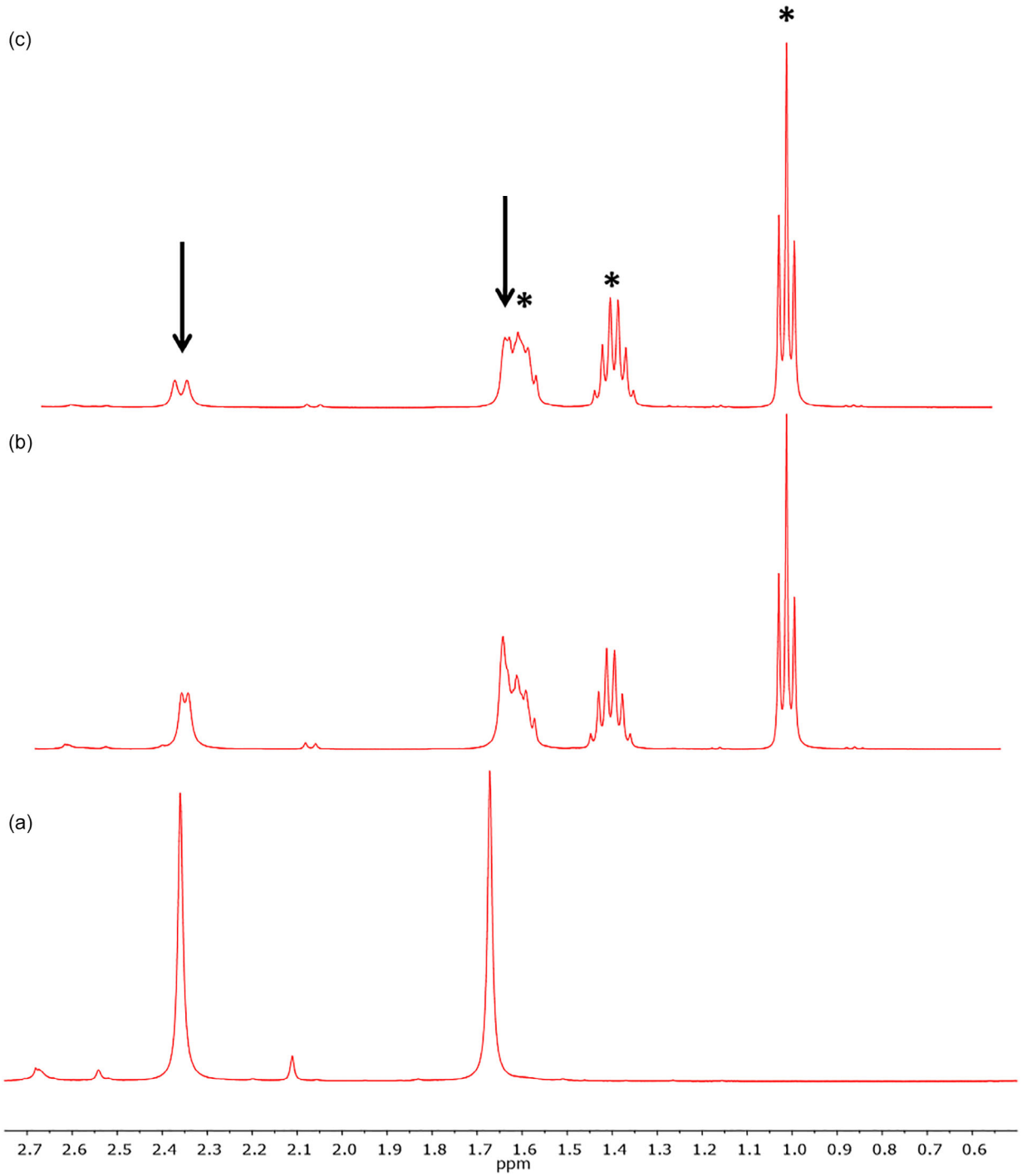

FIGURE 1 | ^{1}H NMR spectra (CD_2Cl_2, 25 °C) of $[Zn(\mathbf{L}^{\mathbf{CH2Py}})_2](ClO_4)_2$ in the (a) absence and (b) presence of 1 equiv. and (c) 2 equiv. of Δ-TRISPHAT. Resonances due to CH_3 groups are indicated by black arrows. Asterisks mark signals due to tetrabutylammonium.

slow diffusion of technical grade methanol in dichloromethane. Two $\mathbf{L}^{\mathbf{CH2Py}}$ molecules are bound to zinc in a *N*,*N*-bidentate mode (Zn—N bond lengths: Zn1—N2 = 2.152(4); Zn1—N4 = 2.044(4); Zn1—N7 = 2.139(4); Zn1—N9 = 2.051(4)), resulting in a N_4O environment around the metal (Figure 4), which thus shows a distorted five-coordinate geometry tending toward trigonal bipyramidal ($\tau_5 = 0.68$ [37]). No Zn···$OClO_3$ interactions are observed, thus excluding the coordination of the anion. In the crystal structure, the two nitrogen atoms of the methylpyridine pendant arms do not coordinate to the zinc(II) center, being involved in hydrogen bonds (O1—H···N1 = 2.822(6) and O1—H···N6 = 2.783(6) Å) with the bound water molecule, contributing to the stabilization of the resulting pentacoordinate species. However, according to the pattern observed in the ^{1}H NMR spectrum, we presume that in solution the pyridine N atoms are coordinated to zinc in $[Zn(\mathbf{L}^{\mathbf{CH2Py}})_2](ClO_4)_2$. Consequently, the metal center has an octahedral geometry, being surrounded by two *N*,*N*,*N*-tridentate $\mathbf{L}^{\mathbf{CH2Py}}$ molecules. The two pyridine N atoms reasonably adopt a *cis* coordination, which could explain the presence of two enantiomers in solution. To further clarify this aspect, DFT calculations were performed by optimizing the geometry of both

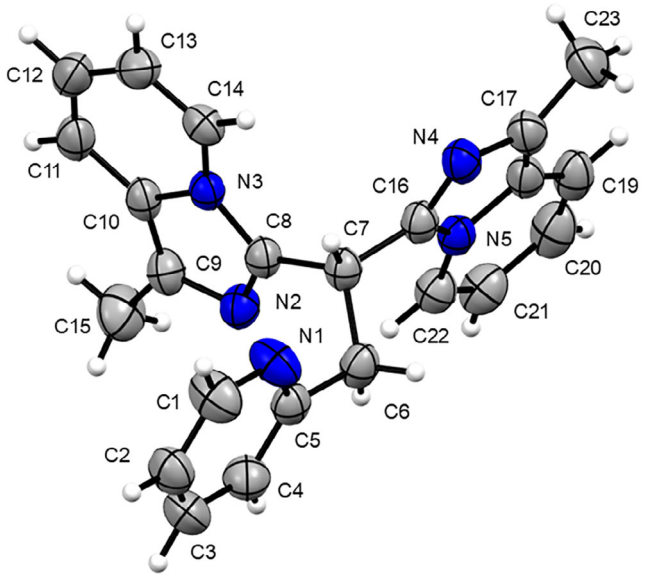

FIGURE 2 | ORTEP representation of $\mathbf{L}^{\mathbf{CH2Py}}$ at 50% probability level ellipsoids, showing the atom labeling scheme.

the *cis* and *trans* isomers that could potentially be generated in complex $[Zn(\mathbf{L}^{\mathbf{CH2Py}})_2](ClO_4)_2$ (vide infra).

2.4 | DFT Calculations

The geometries of representative complexes were optimized at the DFT/PBE0 level of theory. In complex $[Zn(\mathbf{L}^{\mathbf{CH2Py}})Br_2]$ (Figure 5A), the expected tetrahedral coordination is obtained, with ligand $\mathbf{L}^{\mathbf{CH2Py}}$ being *N*,*N*-bidentate and the methylpyridine pendant moiety not coordinated to the zinc(II) center (Zn–Npy = 4.47 Å). As described above, the crystal structure of the complex showed the presence of one water molecule, which affected the orientation of the methyl-pyridinyl group. However, the absence of coordination cannot be ascribed to water but is intrinsic to this system, as supported by DFT calculations. Furthermore, the two methyl groups of the imidazopyridine moiety appear to be nearly equivalent, in agreement with the experimental data (see ^{1}H NMR), also considering that in solution the pyridinic ring is free to rotate.

As stated above, to promote the coordination of the methylpyridine pendant arm to the zinc(II) center, complex $[Zn(\mathbf{L}^{\mathbf{CH2Py}})Br]BF_4$ was synthesized by replacement of one bromide ion. Unfortunately, single crystals suitable for X-ray structural characterization could not be obtained for this species. However, a DFT investigation was performed also on this compound, providing useful information about coordination and symmetry. Geometry optimization resulted in a tetrahedral complex, with the $\mathbf{L}^{\mathbf{CH2Py}}$ ligand bound in *N*,*N*,*N*-tridentate mode and the bromide ion occupying the fourth site. Bond distances are consistent with the described coordination environment (Zn–Br = 2.24 Å; Zn–N1 = 2.02 Å; Zn–N2 = 2.02 Å; Zn–N_{py} = 2.09 Å). Moreover, the complex displays a high degree of symmetry. In particular, the two methyl groups in position 1 appear to be equivalent (Figure 5B, right), the distances between these two methyl groups and the zinc(II) center being respectively 4.91 and 4.92 Å. These observations are in good agreement with the experimental data, since the two methyl groups give rise to a single signal in the ^{1}H NMR spectrum (Figure S9). Additionally, a good agreement between the experimental and calculated stretching in IR spectra of $[Zn(\mathbf{L}^{\mathbf{CH2Py}})Br]^+$ (Figure S20) further supports the proposed structural model and confirms that the DFT calculations provide a reliable description of the coordination environment around the zinc center.

Finally, as mentioned in the previous section, the structure of the cation $[Zn(\mathbf{L}^{\mathbf{CH2Py}})_2]^{2+}$ was optimized as well. The ligand $\mathbf{L}^{\mathbf{CH2Py}}$ can be described as an A_2B-type ligand, where A corresponds to a donor nitrogen atom of the imidazopyridine moiety, while B refers

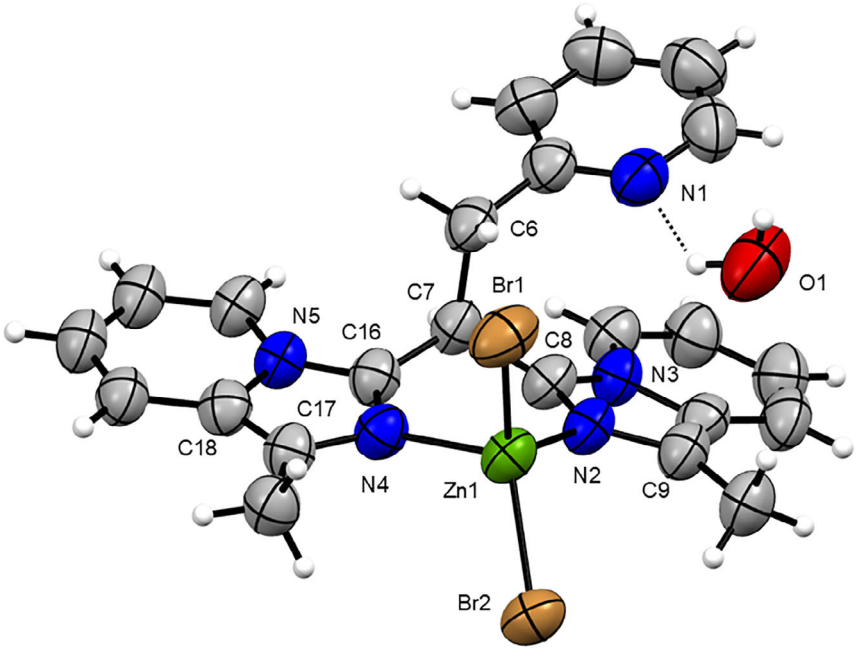

FIGURE 3 | ORTEP representation (50% probability level ellipsoids) of $[Zn(\mathbf{L}^{\mathbf{CH2Py}})Br_2]\cdot H_2O$, showing the intermolecular O—H···N hydrogen bond.

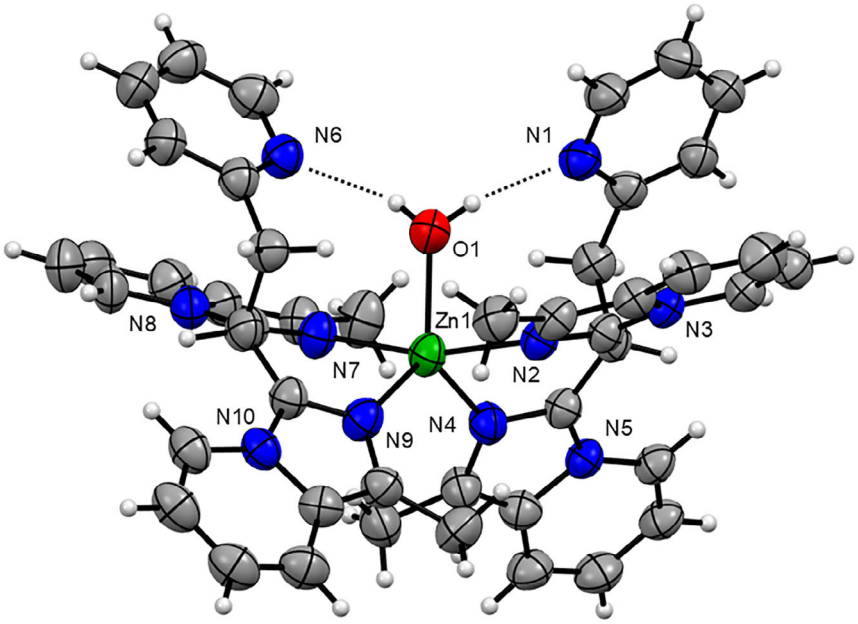

FIGURE 4 | ORTEP representation (30% probability level ellipsoids) of $[Zn(\mathbf{L}^{\mathbf{CH2Py}})_2(OH_2)]^{2+}$, perchlorate anions are omitted for clarity.

to the pyridine nitrogen atom. When two A_2B-type ligands coordinate to a metal center, two isomers may form, commonly defined as *cis* and *trans*, depending on the relative positions of the two B donor atoms. Hypothesizing the coordination of ligand $\mathbf{L}^{\mathbf{CH2Py}}$ as tridentate, the synthesis of $[Zn(\mathbf{L}^{\mathbf{CH2Py}})_2](ClO_4)_2$ can ideally lead to two possible isomers; therefore, geometry optimization was performed for both the *cis* and *trans* isomers (Figure 5C). In the *cis*-$[Zn(\mathbf{L}^{\mathbf{CH2Py}})_2]^{2+}$ cation, the zinc(II) center adopts a slightly distorted octahedral geometry. This type of coordination induces a loss of symmetry: indeed, focusing on the two CH_3 substituents in position 1 of the imidazo[1,5-*a*]pyridine fragments on the same ligand (highlighted in green in Figure 5C), it is evident that their distances from the same pyridinic nitrogen are markedly different. Specifically, the methyl group closer to the nitrogen (top left in the figure) is 3.28 Å away, whereas the more distant methyl group (bottom right in the figure) is 5.86 Å away. A similar observation applies to the methyl groups highlighted in purple, belonging to the other $\mathbf{L}^{\mathbf{CH2Py}}$ ligand, which exhibits the same type of distances. This difference in $CH_3\cdots N_{py}$ distances within the same ligand confirms that the two CH_3 groups in one ligand are not equivalent, thus supporting the ^1H NMR results where the methyl signals showed separate resonances. For the optimized *trans*-$[Zn(\mathbf{L}^{\mathbf{CH2Py}})_2]^{2+}$ cation, the geometry of zinc(II) center is also octahedral, but a higher degree of symmetry is observed. The two CH_3 substituents on the same ligand (Figure 5C, again highlighted in green) exhibit nearly identical distances to the pyridinic nitrogen atom (dashed lines), 5.20 and 5.21 Å, respectively. The same pattern is observed for the methyl groups of the other $\mathbf{L}^{\mathbf{CH2Py}}$ ligand (highlighted in purple). In this case, the CH_3 on the same $\mathbf{L}^{\mathbf{CH2Py}}$ ligand is equivalent and is therefore expected to give rise to a single signal in the ^1H NMR spectrum. DFT calculations also provided the relative energies of the *cis* and *trans* isomers, which were found to be −18078 and −18077 kcal/mol, respectively, so the two isomers are essentially isoenergetic. The predominant formation of the *cis* product under synthetic conditions is likely governed by kinetic factors rather than thermodynamic stability.

The available experimental data (IR and NMR) indicate that the bulk material isolated from the synthesis of $[Zn(\mathbf{L}^{\mathbf{CH2Py}})_2]^{2+}$ does not contain water, and that reasonably, the water molecule found in the crystals comes from technical grade solvents used for crystallization process. However, the isolation of a hydrated five-coordinated structure in the solid state (i.e., $[Zn(\mathbf{L}^{\mathbf{CH2Py}})_2(OH_2)](ClO_4)_2$ could suggest that this is the thermodynamically more stable species in the presence of trace water. Thus, we performed some additional DFT calculations on the hydration process leading from the octahedral *cis*-$[Zn(\mathbf{L}^{\mathbf{CH2Py}})_2]^{2+}$ cation to the five-coordinated aquo-complex observed in the crystal structure (see Supporting Information). The calculated Gibbs free energy change for this reaction is $\Delta G = -1.38$ kcal mol^{-1}, indicating that the process is essentially isoergonic and that neither species is strongly favored on thermodynamic grounds. Therefore, the isolation of the hydrated complex in the single-crystal structure does not necessarily imply that it is the thermodynamically preferred species in solution, even in the presence of trace amounts of water. Rather, we believe that crystallization selectively stabilizes the aquo-complex through packing effects and interactions within the crystal lattice. The good agreement between the experimental and calculated stretchings in IR spectra of $[Zn(\mathbf{L}^{\mathbf{CH2Py}})_2]^{2+}$ (Figure S20) further supports this assumption.

2.5 | Fluorescence Properties

The photophysical data for all compounds are summarized in Table 1, while Figure 6 reports the normalized UV–vis absorption and emission spectra recorded in dichloromethane (5×10^{-5} mol L^{-1}) for the ligand and the complexes. The UV–vis spectrum of the free ligand exhibits two intense absorption bands in the 230–280 nm region, together with a lower-energy absorption centered at 357 nm. The spectral profile closely resembles those of the corresponding zinc complexes; for complexes $[Zn(\mathbf{L}^{\mathbf{CH2Py}})X_2]$ (X = Cl, Br, I), absorptions are not significantly influenced by the halide (Figure S21). However, upon coordination, a

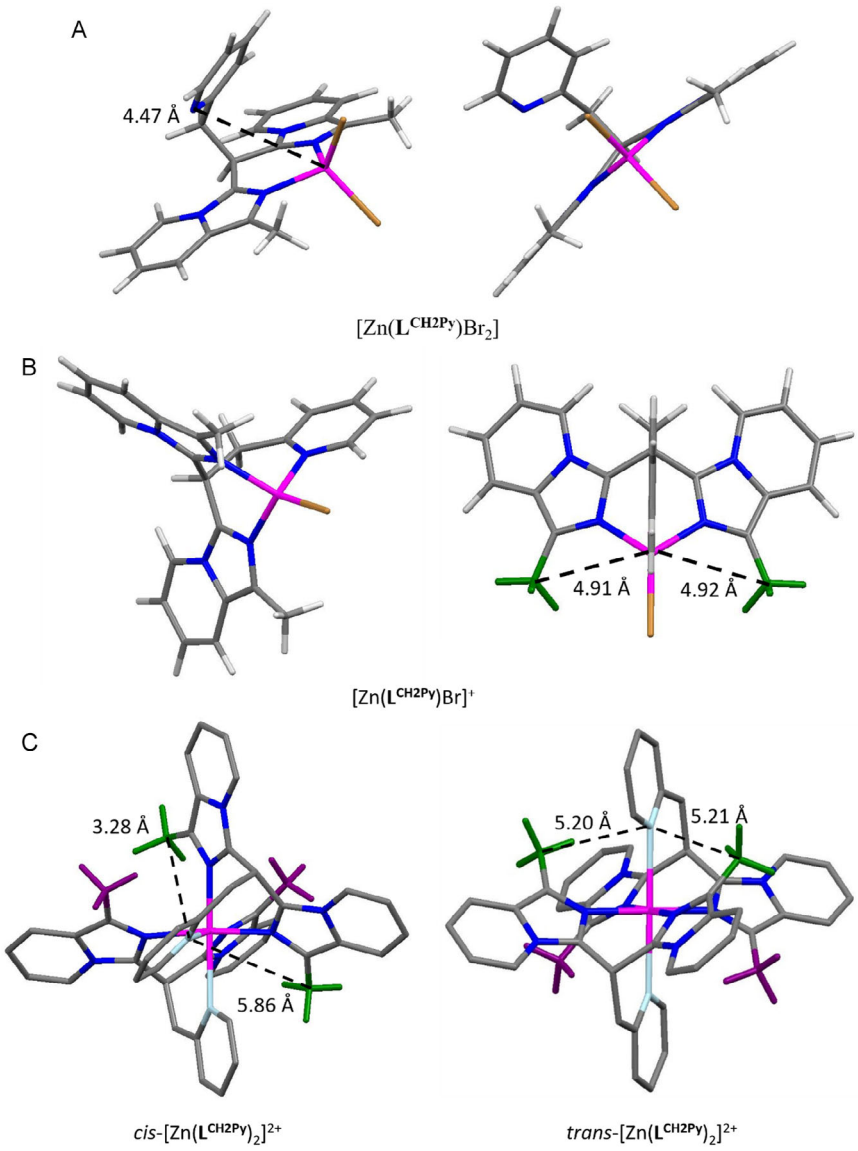

FIGURE 5 | (A) Optimized structure of $[Zn(\mathbf{L}^{\mathbf{CH2Py}})Br_2]$ (Zn, magenta; N, blue; Br, ochre). (B) Optimized structure of $[Zn(\mathbf{L}^{\mathbf{CH2Py}})Br]^+$ (Zn, magenta; N, blue; Br, ochre; CH_3-impy, green). Tetrafluoroborate anion has been omitted for clarity. (C) Optimized structures of *cis*- (left) and *trans*- (right) $[Zn(\mathbf{L}^{\mathbf{CH2Py}})_2]^{2+}$ (Zn, magenta; N, blue; N_{MePy}, light blue; CH_3 groups of ligand 1, green; CH_3 groups of ligand 2, purple). (DFT: PBE0/QZ4P (Zn, Br), TZ2P (N, C), DZP (H)).

hypsochromic shift ($\Delta \approx 20$–35 nm) is observed for both the absorption and the emission bands relative to the free ligand. Because of this coordination-induced blueshift, all zinc(II) derivatives display a blue fluorescence emission, with CIE (x, y) color coordinates close to the standard blue [38] (Figure 6).

All compounds exhibit fluorescence lifetimes in the nanosecond range. The decay profiles of $\mathbf{L}^{\mathbf{CH2Py}}$, $[Zn(\mathbf{L}^{\mathbf{CH2Py}})Cl_2]$, $[Zn\mathbf{L}^{\mathbf{CH2Py}})Br_2]$, and $[Zn(\mathbf{L}^{\mathbf{CH2Py}})I_2]$ are satisfactorily fitted with a mono-exponential function, whereas $[Zn(\mathbf{L}^{\mathbf{CH2Py}})Br]BF_4$ and $[Zn(\mathbf{L}^{\mathbf{CH2Py}})_2](ClO_4)_2$ require a bi-exponential fitting model. Reasonably, the pyridine pendant arm could exhibit dynamic coordination behavior at the metal center that could enhance intramolecular motions and intermolecular interactions, thereby favoring non-radiative decay pathways. Notably, the fluorescence lifetime of $\mathbf{L}^{\mathbf{CH2Py}}$ (5.1 ns) is significantly shorter than that of $\mathbf{L}^{\mathbf{H}}$ and is comparable to those of the corresponding zinc complexes (3.9–10.8 ns). The absolute quantum yields are very high for both the ligand (0.60) and complexes $[Zn(L^{\mathbf{CH2Py}})Cl_2]$ (0.56) and $[Zn(L^{\mathbf{CH2Py}})Br_2]$ (0.50) (Table 1).

The overall similarity between the absorption and emission profiles of free $\mathbf{L}^{\mathbf{CH2Py}}$ and the zinc(II) complexes suggests that the emissive excited state retains a predominantly ligand-centered (^{1}LC) character. This behavior is consistent with the d^{10} electronic configuration of zinc(II), which does not provide low-lying metal-centered excited states capable of efficiently competing with ligand fluorescence. Consequently, metal coordination mainly affects the photophysical response through geometric and electronic perturbations of the ligand framework, rather than by introducing new emissive pathways. In the present case, coordination induces a moderate hypsochromic shift of both absorption and emission bands, while preserving the high quantum yields observed for the free ligand. This indicates that

TABLE 1 | Photophysical data for ligands $\mathbf{L^H}$ and $\mathbf{L^{CH2Py}}$ and complexes $[Zn(\mathbf{L^{CH2Py}})_2X_2]$ (X = Cl, Br, I), $[Zn(\mathbf{L^{CH2Py}})Br]BF_4$, and $[Zn(\mathbf{L^{CH2Py}})_2](ClO_4)_2$ in solution (CH_2Cl_2, $5 \cdot 10^{-5}$ M).

	λ_{abs}, nm	λ_{exc}, nm	λ_{em}, nm	ΔStokes, eV	Φ_{PL}	τ, ns
$\mathbf{L^H}$	356[a]	356[a]	450[a]	0.73[a]	0.84[a]	19.7[a]
$\mathbf{L^{CH2Py}}$	357	357	453	0.74	0.60	5.1
$[Zn(\mathbf{L^{CH2Py}})Cl_2]$	339	339	437	0.82	0.56	10.8
$[Zn(\mathbf{L^{CH2Py}})Br_2]$	338	341	436	0.83	0.50	7.8
$[Zn(\mathbf{L^{CH2Py}})I_2]$	340	339	437	0.81	0.22	3.9
$[Zn(\mathbf{L^{CH2Py}})Br]BF_4$	332	335	424	0.81	0.38	7.6[b]
$[Zn(\mathbf{L^{CH2Py}})_2](ClO_4)_2$	330	333	419	0.80	0.22	4.1[b]

[a]From Ref. [34].
[b]Weighted average of a biexponential decay. $[Zn(\mathbf{L^{CH2Py}})Br]BF_4$: $\tau_1 = 3.8$ (14.25%), $\tau_2 = 8.2$ (85.75%). $[Zn(L^{CH2Py})_2](ClO_4)_2$: $\tau_1 = 1.9$ (43.12%), $\tau_2 = 5.8$ (56.88%).

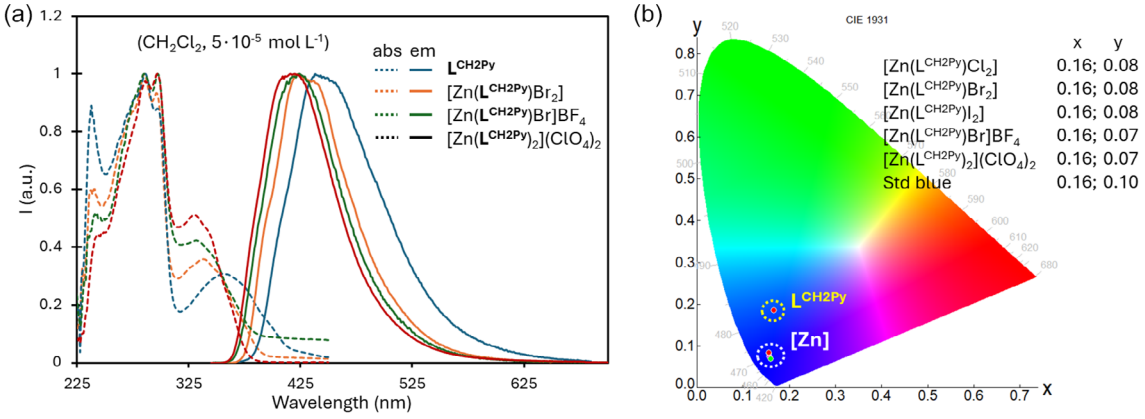

FIGURE 6 | (a) Normalized absorption (dashed lines) and emission (full lines) spectra of ligand L^{CH2Py} and complexes recorded in solution (CH_2Cl_2, $5 \cdot 10^{-5}$ mol L^{-1}). (b) Chromaticity plot (CIE 1931) for ligand $\mathbf{L^{CH2Py}}$ and complexes in solution (CH_2Cl_2, $5 \cdot 10^{-5}$ mol L^{-1}). Top right: (x, y) color coordinates for zinc complexes, compared with standard blue.

zinc(II) acts primarily as a structural modulator, maintaining the intrinsic fluorescence of the bis(imidazo[1,5-*a*]pyridine)methane ligand while tuning its emission toward the blue region. Additionally, TD-DFT calculations were performed to gain further insight into the nature of the emissive excited state (S_1). Figure 7 reports the natural transition orbitals (NTOs) and electron density difference maps (EDDMs) for the cation $[Zn(\mathbf{L^{CH2Py}})_2Br]^+$, taken as a representative example. NTOs and EDDMs for the other complexes are reported in the Supporting Information (Figure S22).

Analysis of the NTOs associated with the S_1 state reveals that both the virtual and occupied orbitals are almost entirely localized on the ligand framework, with negligible contribution from the zinc center (Figure 7, left). Consistently, the corresponding EDDMs plots (Figure 7, right) show that the electron-density redistribution upon excitation is confined to the ligand scaffold. These results confirm that the lowest excited state (S_1) possesses a predominantly ligand-centered character, explaining the close similarity between the photophysical properties of the free ligand and the zinc(II) complexes.

Overall, these fluorescent features are consistent with those observed for the corresponding complexes with the parent Bis (imidazo[1,5-*a*]pyridine)methane *N*,*N*-bidentate ligand ($\mathbf{L^H}$) [34].

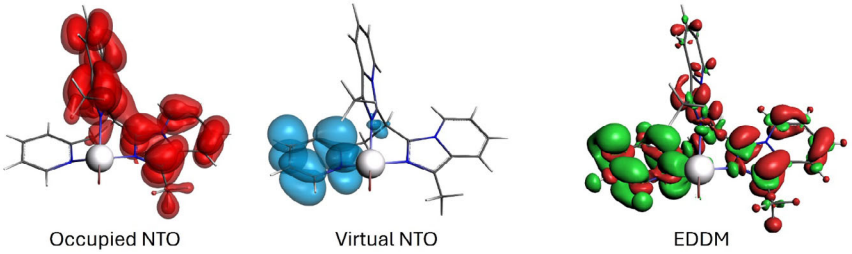

FIGURE 7 | Natural transition orbitals (NTOs) (left) and electron density difference maps (EDDMs) (right) calculated for the first singlet excited state (S_1) for cation $[Zn(\mathbf{L^{CH2Py}})_2Br]^+$ (DFT: PBE0// QZ4P (Zn, Br), TZ2P (N, C), TZP (H)).

3 | Conclusions

In this work, we extended our previous investigation on bis(imidazo[1,5-*a*]pyridine)methane ligands by introducing a methylpyridine pendant arm on the ligand framework, thus obtaining a tripodal *N*,*N*,*N*-tridentate ligand. This ligand was successfully coordinated to zinc(II) centers, affording mononuclear complexes that were fully characterized from both structural and spectroscopic viewpoints. Notably, the tridentate coordination mode in $[Zn(\mathbf{L^{CH2Py}})_2](ClO_4)_2$ imposes a *cis* arrangement around the metal center, leading to the formation of a couple of enantiomers, as supported both by NMR analysis and DFT calculations. The photophysical investigation revealed that these zinc(II) complexes exhibit intense blue fluorescence, with emission profiles comparable to those observed in the earlier series, confirming that the introduction of an additional donor arm does not compromise the emissive properties of the system. On the contrary, the increased rigidity and defined coordination environment provided by the tripodal ligands may represent a valuable feature for the development of advanced luminescent materials. Overall, this study further expands the scope of bis(imidazo[1,5-*a*]pyridine)-based ligands in coordination chemistry, demonstrating their versatility in accessing structurally diverse and luminescent zinc(II) complexes, including chiral species of potential interest for circularly polarized luminescence (CPL) applications. Future work will focus on the resolution of the racemic mixtures and on the isolation and detailed investigation of the fluorescence properties of the individual enantiomers.

4 | Experimental Section

4.1 | General Information

Infrared spectra were acquired on a Shimadzu Prestige-21 spectrometer with a 1 cm^{-1} resolution. Elemental analyses were obtained with a Perkin-Elmer CHN Analyzer 2400 Series II. NMR spectra were recorded with an AVANCE 400 Bruker spectrometer operating at 400 MHz for ^1H NMR and 100 MHz for APT $^{13}C\{^1H\}$ NMR. Chemical shifts are given as δ values in ppm relative to residual solvent peaks as the internal reference. *J* values are given in Hz. The UV–vis, excitation, and emission spectra were measured using a fluorescence spectrometer (Edinburgh Instruments FS5) equipped with a 150 W continuous Xenon lamp as a light source and a detector for transmittance. All spectra were corrected for the wavelength response of the instrument; lifetime measurements were performed on the same FS5 Edinburgh Instruments equipped with an EPLED-320 (Edinburgh Instruments) as the pulsed source. Analysis of the lifetime decay curves was done using Fluoracle Software package (Ver. 1.9.1), which runs the FS5 instrument. Absolute fluorescence quantum yields were determined on a Photon Technology International (PTI) QuantaMaster QM-40 spectrometer (Xe arc lamp, 75 W) with a PhotoMed GmbH K-Sphere Integrating Sphere (3.2 inch. diameter). All chemicals have been purchased (TCI Chemicals, Fluorochem, Carlo Erba) and used without further purification. Bis(1-methylimidazo[1,5-*a*]pyridin-3-yl)methane ($\mathbf{L^H}$) was prepared as previously reported [34].

4.2 | Synthesis of 2-Chloromethylpyridine

2-Chloromethylpyridine is commonly stored in its hydrochloride form to enhance its stability. 2-(Chloromethyl)pyridine hydrochloride (1.00 g, 6.10 mmol) was dissolved in water (10 mL), and K_2CO_3 (1.69 g, 12.20 mmol) was carefully added in small portions. The reaction mixture was stirred for 15 min, after which dichloromethane (20 mL) was added and stirring was continued for an additional 15 min. Then 50 mL of water was added, and the layers were separated. The aqueous phase was extracted with dichloromethane (3 × 50 mL). The combined organic layers were dried over anhydrous Na_2SO_4, filtered, and concentrated under reduced pressure to afford a red liquid, which was used without further purification. Yield: 0.73 g (92%). ^1H NMR (400 MHz, $CDCl_3$, 298 K, *J* [Hz]): $\delta = 8.58$ (d, $J = 4.5$ Hz, 1H), 7.72 (td, $J = 7.7$, 1.6 Hz, 1H), 7.47 (d, $J = 7.8$ Hz, 1H), 7.34–7.04 (m, 1H), 4.68 (s, 2H). $^{13}C\{^1H\}$ NMR (100 MHz, CD_2Cl_2, 298 K): δ 156.3, 149.2, 136.8, 122.8, 122.6, 46.6. NMR data (Figures S23 and S24) are consistent with those reported in the literature [39].

4.3 | Synthesis of 3,3′-(2-Pyridylethane-1,1-diyl) bis(1-methylimidazo[1,5-*a*]pyridine) ($\mathbf{L^{CH2Py}}$)

A solution of methylmagnesium bromide (4 mL of a 3 M solution in diethyl ether, 12 mmol) diluted in diisopropyl ether (5 mL) was added dropwise at room temperature to a suspension of $\mathbf{L^H}$ (1.5 g, 5.43 mmol) in diisopropyl ether (15 mL). After complete addition, the reaction mixture was refluxed and stirred for 4 h under an inert atmosphere. After cooling to room temperature, 2-chloromethylpyridine (16.30 mmol) was added slowly. The resulting red suspension was stirred at 55 °C for an additional 12 h. The reaction was quenched with an aqueous NH_4Cl solution (150 mL), and the organic layer was extracted with dichloromethane (3 × 100 mL). The combined organic extracts were dried over anhydrous Na_2SO_4, filtered, and the solvent was removed under reduced pressure. The crude residue was dissolved in diethyl ether (10 mL), and the suspension was filtered to remove any unreacted $\mathbf{L^H}$. Concentration of the filtrate under vacuum afforded a yellow-to-orange solid. Yield: 1.12 g (56%). Anal. Calcd (%) for $C_{23}H_{21}N_5$: C, 75.18; H, 5.76; N, 19.06. Found (%): C, 74.80; H, 5.70; N, 18.79. ^1H NMR (400 MHz, CD_2Cl_2, 298 K, *J* [Hz]): $\delta = 8.46$ (d, $J = 4.4$ Hz, 1H), 7.87 (t, $J = 9.0$ Hz, 2H), 7.50–7.36 (m, 1H), 7.27 (d, $J = 9.2$ Hz, 2H), 7.11–6.97 (m, 2H), 6.58–6.44 (m, 2H), 6.36 (t, $J = 6.7$ Hz, 2H), 5.53 (t, $J = 7.5$ Hz, 1H), 3.95 (d, $J = 7.5$ Hz, 2H), 2.44 (s, 6H). $^{13}C\{^1H\}$ NMR (100 MHz, CD_2Cl_2, 298 K): $\delta = 159.6$, 149.7, 136.5, 134.9, 127.9, 127.3, 124.3, 122.0, 121.7, 118.4, 116.9, 112.5, 39.1, 38.0, 12.8. IR: $\nu_{C=N} = 1640\ cm^{-1}$.

4.4 | Syntheses of $[Zn(\mathbf{L^{CH2Py}})X_2]$ Complexes

Zinc(II) halide (ZnX_2, X = Cl, Br, I) (0.40 mmol) was added to a solution of ligand $\mathbf{L^{CH2Py}}$ (150 mg, 0.40 mmol) in methanol (15 mL), and the reaction mixture was stirred at room temperature for 4 h under an inert atmosphere. A suspension was formed, and the product was collected by filtration and washed with diethyl ether, affording a pale yellow solid.

4.4.1 | $[Zn(\mathbf{L}^{\mathbf{CH2Py}})Cl_2]$

Yield: 139 mg (70.0%). Anal. Calcd (%) for $C_{23}H_{21}Cl_2N_5Zn$: C, 54.84; H, 4.20; N, 13.90. Found (%): C, 54.68; H, 4.19; N, 13.60. ^{1}H NMR (400 MHz, CD_2Cl_2, 298 K, J [Hz]): $\delta = 8.59$ (d, $J = 4.4$ Hz, 1H), 7.95 (d, $J = 7.2$ Hz, 2H), 7.41 (d, $J = 9.2$ Hz, 2H), 7.33 (td, $J = 7.6$, 1.5 Hz, 1H), 7.08 (dd, $J = 7.1$, 5.2 Hz, 1H), 6.78–6.69 (m, 3H), 6.64 (t, $J = 6.7$ Hz, 2H), 5.76 (t, $J = 7.5$ Hz, 1H), 3.56 (d, $J = 7.5$ Hz, 2H), 2.75 (s, 6H). ^{13}C{^{1}H} NMR (100 MHz, CD_2Cl_2, 298 K): $\delta = 156.8$, 150.1, 137.6, 134.0, 128.5, 127.4, 124.7, 123.1, 120.9, 119.4, 118.9, 115.5, 44.9, 33.4, 12.2. IR: $\nu_{C=N} = 1648\ cm^{-1}$.

4.4.2 | $[Zn(\mathbf{L}^{\mathbf{CH2Py}})Br_2]$

Yield: 227 mg (83.0%). Anal. Calcd (%) for $C_{23}H_{21}Br_2N_5Zn$: C, 46.61; H, 3.57; N, 11.82. Found (%): C, 46.40; H, 3.60; N, 11.61. ^{1}H NMR (400 MHz, CD_2Cl_2, 298 K, J [Hz]): $\delta = 8.58$ (d, $J = 4.4$ Hz, 1H), 7.96 (d, $J = 7.2$ Hz, 2H), 7.42 (d, $J = 9.2$ Hz, 2H), 7.32 (td, $J = 7.6$, 1.7 Hz, 1H), 7.08 (dd, $J = 6.9$, 5.1 Hz, 1H), 6.78–6.68 (m, 3H), 6.65 (dd, $J = 10.0$, 3.5 Hz, 2H), 5.79 (t, $J = 7.6$ Hz, 1H), 3.55 (d, $J = 7.6$ Hz, 2H), 2.79 (s, 6H). ^{13}C{^{1}H} NMR (100 MHz, CD_2Cl_2, 298 K): $\delta = 156.7$, 150.1, 137.6, 133.8, 128.6, 127.5, 124.7, 123.1, 120.8, 119.5, 118.9, 115.6, 44.9, 33.6, 12.6. IR: $\nu_{C=N} = 1655\ cm^{-1}$.

4.4.3 | $[Zn(\mathbf{L}^{\mathbf{CH2Py}})I_2]$

Yield: 210 mg (87.0%). Anal. Calcd (%) for $C_{23}H_{21}I_2N_5Zn$: C, 40.23; H, 3.08; N, 10.20. Found (%): C, 40.02; H, 3.15; N, 9.91. ^{1}H NMR (400 MHz, CD_2Cl_2, 298 K, J [Hz]): $\delta = 8.60$ (d, $J = 4.4$ Hz, 1H), 7.92 (d, $J = 7.3$ Hz, 2H), 7.47 (t, $J = 19.1$ Hz, 2H), 7.36–7.24 (m, 1H), 7.09 (dd, $J = 7.0$, 5.2 Hz, 1H), 6.75 (dd, $J = 9.1$, 6.5 Hz, 2H), 6.66 (dd, $J = 14.2$, 7.2 Hz, 3H), 5.81 (t, $J = 7.4$ Hz, 1H), 3.50 (d, $J = 7.4$ Hz, 2H), 2.86 (s, 6H). ^{13}C{^{1}H} NMR (100 MHz, CD_2Cl_2, 298 K): $\delta = 156.6$, 150.2, 137.6, 133.7, 128.7, 127.9, 124.6, 123.2, 120.8, 119.5, 118.9, 115.7, 44.7, 33.9, 13.2. IR: $\nu_{C=N} = 1652\ cm^{-1}$.

4.5 | Syntheses of $[Zn(L^{CH2Py})Br]BF_4$

$NaBF_4$ (38.84 mg, 0.35 mmol) and $AgNO_3$ (60.10 mg, 0.35 mmol) were dissolved in CH_3CN (5 mL), and the reaction mixture was stirred for 45 min at room temperature, in the dark. A white solid ($NaNO_3$) formed, was removed by filtration, and washed with CH_3CN. The resulting filtrate, containing $AgBF_4$, was added to a solution of complex $[Zn(L^{CH2Py})Br_2]$ (150 mg, 0.26 mmol), and the reaction mixture was stirred for 1.5 h at room temperature, under inert atmosphere, in the dark. A suspension formed, and the solid (AgBr) was removed by filtration and washed with CH_3CN. The filtrate was concentrated by reduced pressure to afford an oil. The residue was triturated with diethyl ether, and the resulting precipitate was collected by filtration to give the product as a pale yellow solid. Yield: 129 mg (90.0%). Anal. Calcd (%) for $C_{23}H_{21}BBrF_4N_5Zn$: C, 46.08; H, 3.53; N, 11.68. Found (%): C, 45.71; H, 3.45; N, 11.30. ^{1}H NMR (400 MHz, CD_3CN, 298 K, J [Hz]): $\delta = 8.74$ (s, 1H), 8.30 (t, $J = 22.1$ Hz, 2H), 7.85 (t, $J = 7.4$ Hz, 1H), 7.64–7.50 (m, 2H), 7.51–7.39 (m, 1H), 7.15 (d, $J = 7.5$ Hz, 1H), 6.93 (dd, $J = 6.5$, 2.7 Hz, 4H), 5.85 (t, $J = 5.3$ Hz, 1H), 3.73 (d, $J = 5.3$ Hz, 2H), 2.60 (s, 6H). ^{13}C{^{1}H} NMR (100 MHz, CD_3CN, 298 K): $\delta = 155.9$, 151.7, 140.8, 134.4, 128.8, 128.3, 127.6, 124.7, 122.6, 121.1, 119.2, 116.6, 38.6, 31.0, 11.8. IR: $\nu_{C=N} = 1650\ cm^{-1}$, $\nu_{BF4} = 1100\ cm^{-1}$.

4.6 | Synthesis of $[Zn(L^{CH2Py})_2](ClO_4)_2$

Zinc(II) perchlorate hexahydrate (70.0 mg, 0.19 mmol) was added to a solution of ligand (150 mg, 0.41 mmol) in 10 mL of methanol, and the mixture was stirred at room temperature for 5 h. A suspension was formed, and the yellow solid was filtered off, washed with diethyl ether, and dried under vacuum. Yield: 148 mg (80.0%). Anal. Calcd (%) for $C_{46}H_{42}Cl_2N_{10}O_8Zn$: C, 55.30; H, 4.24; N, 14.02. Found (%): 54.89; H, 4.33; N, 13.69. ^{1}H NMR (400 MHz, CD_2Cl_2, 298 K, J [Hz]): $\delta = 8.79$ (d, $J = 6.6$ Hz, 2H), 8.24 (t, $J = 12.2$ Hz, 2H), 8.07 (d, $J = 4.5$ Hz, 2H), 7.77 (d, $J = 7.8$ Hz, 2H), 7.65 (tt, $J = 15.7$, 7.9 Hz, 2H), 7.36 (dd, $J = 19.7$, 9.2 Hz, 4H), 7.04 (dd, $J = 6.9$, 5.4 Hz, 2H), 6.93 (dd, $J = 17.2$, 8.0 Hz, 4H), 6.81–6.73 (m, 2H), 6.68 (t, $J = 6.3$ Hz, 2H), 6.32 (t, $J = 8.1$ Hz, 2H), 3.97–3.70 (m, 4H), 2.41 (s, 6H), 1.65 (s, 6H). ^{13}C{^{1}H} NMR (100 MHz, CD_2Cl_2, 298 K): $\delta = 155.9$, 148.8, 138.6, 135.7, 134.2, 128.2, 127.9, 126.7, 126.4 126.2, 123.3, 122.9, 122.2, 121.4, 120.7, 118.1, 117.2, 116.7, 115.8, 44.6, 33.3, 12.4, 11.1. IR: $\nu_{C=N} = 1650\ cm^{-1}$, $\nu_{ClO4} = 1070\ cm^{-1}$.

4.7 | X-Ray Structure Determination

Crystals of $\mathbf{L}^{\mathbf{CH2Py}}$, $[Zn(\mathbf{L}^{\mathbf{CH2Py}})Br_2]\cdot H_2O$, and $[Zn(\mathbf{L}^{\mathbf{CH2Py}})_2(OH_2)](ClO_4)_2$ were obtained by slow evaporation of a concentrated diethylether solution ($\mathbf{L}^{\mathbf{CH2Py}}$), by slow diffusion of hexane into an acetone solution ($[Zn(\mathbf{L}^{\mathbf{CH2Py}})Br_2]\cdot H_2O$) and slow diffusion of methanol into a dichloromethane solution ($[Zn(\mathbf{L}^{\mathbf{CH2Py}})_2(OH_2)](ClO_4)_2$). All crystals were mounted on a STOE STADIVARI Eulerian 4-circle diffractometer equipped with a Pilatus300K detector, using Cu-Kα radiation (λ = 1.54186 Å). The structures were solved and refined by direct methods using the OLEX2 platform [40]. The H-atoms were included in calculated positions and treated as riding atoms, while the non-H atoms were refined anisotropically, using weighted full-matrix least-square on F^2. Crystallographic details are summarized in Table S2. Figures 2–4 were drawn with Mercury [41]. In $[Zn(\mathbf{L}^{\mathbf{CH2Py}})_2(OH_2)](ClO_4)_2$ a void of 71 Å^3 (≈20 electrons) was observed. This void was considered to be a highly disordered methanol molecule retained in the crystal growth process, and it was removed during refinement using the Mask algorithm from OLEX2, thus explaining the alerts-A associated to this structure. Nevertheless, the structure of the complex is sound, and it confirms the formation of the penta-coordinated complex during the crystallization process.

CCDC-2549139 ($\mathbf{L}^{\mathbf{CH2Py}}$), 2549140 ($[Zn(\mathbf{L}^{\mathbf{CH2Py}})Br_2]\cdot H_2O$), and 2549141 ($[Zn(\mathbf{L}^{\mathbf{CH2Py}})_2(OH_2)](ClO_4)_2$) contain the supplementary crystallographic data for this paper. These data can be obtained free of charge via www.ccdc.cam.ac.uk/data_request/cif, by e-mailing data_request@ccdc.cam.ac.uk, or by contacting The Cambridge Crystallographic Data Centre, 12, Union Road, Cambridge CB2 1EZ, UK; fax: +44 1223 336033.

4.8 | Computational Details

All calculations were carried out at the density functional level of theory with the ADF2022.101 program package [42–44]. The PBE0 functional [45] was employed for all calculations. Frequency analyses were performed for all optimized structures to establish the nature of the stationary points. For geometry optimizations, C and N atoms were described through TZ2P basis sets [triple-ξ Slater-type orbitals (STOs) plus two polarization functions], Zn and Br atoms were described through QZ4P basis sets [quadruple-ξ STOs plus four polarization functions], and H atoms were described through DZP basis sets [double-ξ STOs plus one polarization function]. Restricted formalism, no-frozen-core approximation (all-electron), and no-symmetry constraints were used in all calculations. Solvent effects (CH_2Cl_2) were simulated employing the conductor-like continuum solvent model (COSMO) [46–48] as implemented in the ADF suite.

Author Contributions

Gioele Colombo: methodology, investigation, data curation, writing – original draft preparation. **Anita Cinco:** methodology, investigation, data curation. **Chiara Vola:** methodology, investigation, data curation, writing – original draft preparation. **Bruno Therrien:** methodology, investigation, data curation, writing – review and editing. **Stefano Brenna:** Conceptualization, methodology, supervision, funding acquisition, writing – original draft preparation. **G. Attilio Ardizzoia:** conceptualization, software, supervision, funding acquisition, writing – review and editing.

Acknowledgments

The authors thank the Ministero dell'Università e della Ricerca (MUR) and the University of Insubria for funding. Scientific support from CRIETT Center of University of Insubria (instruments code: MAC-01, -04, -06, -12, -13) is greatly acknowledged.

Open access publishing facilitated by Universita degli Studi dell'Insubria, as part of the Wiley - CRUI-CARE agreement.

Funding

This study was supported by Ministero dell'Università e della Ricerca, Università degli Studi dell'Insubria.

Conflicts of Interest

The authors declare no conflicts of interest.

Data Availability Statement

The data that support the findings of this study are available from the corresponding author upon reasonable request.

References

1. J. Taut, J.-C. Chambron, and B. Kersting, "Fifty Years of Inorganic Biomimetic Chemistry: From the Complexation of Single Metal Cations to Polynuclear Metal Complexes by Multidentate Thiolate Ligands," *European Journal of Inorganic Chemistry* 26 (2023): e202200739.

2. C. Sappino, S. Di Stefano, O. Lanzalunga, C. Zonta, and G. Licini, "Transition Metal Catalysts Bearing Multidentate Ligands for Efficient and Environmental Benign Oxidations by H_2O_2," *European Journal of Inorganic Chemistry* 26 (2023): e202200782.

3. C.-W. Lu, Y. Wang, and Y. Chi, "Metal Complexes with Azolate-Functionalized Multidentate Ligands: Tactical Designs and Optoelectronic Applications," *Chemistry – A European Journal* 22 (2016): 17892–17908.

4. B. Carr, C. L. Fleming, and A. G. Blackman, "Syntheses and Structures of Transition Metal Complexes of Quinoline-Containing Multidentate Amine Ligands," *Coordination Chemistry Reviews* 502 (2024): 215599.

5. M. Raulin, G. Licini, and C. Zonta, "Tris(2-Pyridylmethyl)amines-Based Metal Complexes as Versatile Scaffold in Catalysis," *Coordination Chemistry Reviews* 551 (2026): 217417.

6. D. Saren, E. Zangrando, H. Puschmann, and S. C. Manna, "Tridentate Chelating Ligand Based Fluorescent Zn(Ii) Coordination Compounds for Highly Selective Detection of Picric Acid," *New Journal of Chemistry* 48 (2024): 4821–4830.

7. B. Panunzi, R. Diana, S. Concilio, et al., "Fluorescence pH-Dependent Sensing of Zn(II) by a Tripodal Ligand. A Comparative X-Ray and DFT Study," *Journal of Luminescence* 212 (2019): 200–206.

8. G. Colombo, G. A. Ardizzoia, and S. Brenna, "Imidazo[1,5-a]pyridine-Based Derivatives as Highly Fluorescent Dyes," *Inorganica Chimica Acta* 535 (2022): 120849.

9. X. Kong, J. Zhao, L. Yang, F. Wang, and Z. Sun, "A Novel 2-(2-Aminophenyl) Imidazo [1,5-a] Pyridine-Based Fluorescent Probe for Rapid Detection of Phosgene," *Analytical and Bioanalytical Chemistry* 416 (2024): 329–339.

10. R. Cui, C. Liu, P. Zhang, K. Qin, and Y. Ge, "An Imidazo[1,5-a]pyridine Benzopyrylium-Based NIR Fluorescent Probe with Ultra-Large Stokes Shifts for Monitoring SO2," *Molecules* 28 (2023): 515.

11. J. D. Girase, A. B. Kajjam, D. K. Dubey, K. K. Kesavan, J.-H. Jou, and S. Vaidyanathan, "Unipolar 1-Phenylimidazo[1,5- *a*]pyridine: A New Class of Ultra-Bright Sky-Blue Emitters for Solution-Processed Organic Light Emitting Diodes," *New Journal of Chemistry* 46 (2022): 16717–16729.

12. L. Valla, D. Pitrat, J.-C. Mulatier, et al., "Imidazo[1,2- *a*]pyridine and Imidazo[1,5- *a*]pyridine: Electron Donor Groups in the Design of D–π–A Dyes," *The Journal of Organic Chemistry* 89 (2024): 8407–8419.

13. M. R. Reddy, C. M. Darapaneni, R. D. Patil, and H. Kumari, "Recent Synthetic Methodologies for Imidazo[1,5- *a*]pyridines and Related Heterocycles," *Organic & Biomolecular Chemistry* 20 (2022): 3440–3468.

14. G. Volpi, "Luminescent Imidazo[1,5- *a*]pyridine Scaffold: Synthetic Heterocyclization Strategies-Overview and Promising Applications," *Asian Journal of Organic Chemistry* 11 (2022): e202200171.

15. A. Cinco, C. Vola, G. A. Ardizzoia, S. Brenna, and G. Colombo, "Nitrogen Position Matters: Synthetic Strategies, Functional Behavior and Dual Roles in Medicine and Materials in the Imidazopyridine Family," *Applied Sciences* 16 (2026): 1937.

16. A. Joshi, D. Chandra Mohan, and S. Adimurthy, "Copper-Catalyzed Denitrogenative Transannulation Reaction of Pyridotriazoles: Synthesis of Imidazo[1,5- *a*]pyridines with Amines and Amino Acids," *Organic Letters* 18 (2016): 464–467.

17. A. Cinco, G. A. Ardizzoia, S. Brenna, B. Therrien, and G. Colombo, "Boron-Centered Compounds: Exploring the Optical Properties of Spiro Derivatives with Imidazo[1,5-a]Pyridines," *Molecules* 30 (2025): 2552.

18. F. Yagishita, K. Hoshi, S. Mukai, et al., "Effect of Phenolic Substituent Position in Boron Complexes of Imidazo[1,5- *a*]pyridine," *Asian Journal of Organic Chemistry* 11 (2022): e202200040.

19. G. Colombo, G. A. Ardizzoia, J. Furrer, B. Therrien, and S. Brenna, "Driving the Emission Towards Blue by Controlling the HOMO-LUMO Energy Gap in BF_2 -Functionalized 2-(Imidazo[1,5- *a*]pyridin-3-yl)phenols," *Chemistry – A European Journal* 27 (2021): 12380–12387.

20. G. Colombo, A. Romeo, G. A. Ardizzoia, J. Furrer, B. Therrien, and S. Brenna, "Boron Difluoride Functionalized (tetrahydroimidazo[1,5-a]

pyridin-3-Yl)phenols: Highly Fluorescent Blue Emissive Materials," *Dyes and Pigments* 182 (2020): 108636.

21. V. Cerrato, G. Volpi, E. Priola, et al., "Mono-, Bis-, and Tris-Chelate Zn(II) Complexes with Imidazo[1,5-a]pyridine: Luminescence and Structural Dependence," *Molecules* 28 (2023): 3703.

22. P. Pinter, R. Pittkowski, J. Soellner, and T. Strassner, "The Chameleonic Nature of Platinum(II) Imidazopyridine Complexes," *Chemistry – A European Journal* 23 (2017): 14173–14176.

23. G. Colombo, A. Cinco, J. Furrer, B. Therrien, S. Brenna, and G. A. Ardizzoia, "Luminescent Blue Emissive Bis(alkynyl) Borane Compounds with a N,O-Coordinated Ligand," *Dyes and Pigments* 220 (2023): 111722.

24. N. Kundu, M. Maity, P. B. Chatterjee, S. J. Teat, A. Endo, and M. Chaudhury, "Reporting a Unique Example of Electronic Bistability Observed in the Form of Valence Tautomerism with a Copper(II) Helicate of a Redox-Active Nitrogenous Heterocyclic Ligand," *Journal of the American Chemical Society* 133 (2011): 20104–20107.

25. A. L. Guckian, M. Doering, M. Ciesielski, et al., "Assessment of Intercomponent Interaction in Phenylene Bridged Dinuclear Ruthenium(ii) and Osmium(ii) Polypyridyl Complexes," *Dalton Transactions* 33 (2004): 3943–3949.

26. N. Kundu, S. M. T. Abtab, S. Kundu, A. Endo, S. J. Teat, and M. Chaudhury, "Triple-Stranded Helicates of Zinc(II) and Cadmium(II) Involving a New Redox-Active Multiring Nitrogenous Heterocyclic Ligand: Synthesis, Structure, and Electrochemical and Photophysical Properties," *Inorganic Chemistry* 51 (2012): 2652–2661.

27. M. E. Bluhm, C. Folli, D. Pufky, M. Kröger, O. Walter, and M. Döring, "3-Aminoiminoacrylate, 3-Aminoacrylate, and 3-Amidoiminomalonate Complexes as Catalysts for the Dimerization of Olefins," *Organometallics* 24 (2005): 4139–4152.

28. S. Panda, S. K. Bera, P. Goel, A. K. Dutta, and G. K. Lahiri, "Ruthenium-Chelated Non-Innocent Bis(heterocyclo)methanides: A Mimicked β-Diketiminate," *Inorganic Chemistry* 58 (2019): 11458–11469.

29. S. Panda, R. Baliyan, S. Dhara, K.-W. Huang, and G. K. Lahiri, "Redox Induced Oxidative C–C Coupling of Non-Innocent Bis(heterocyclo)methanides," *Dalton Transactions* 50 (2021): 16647–16659.

30. S. Tahara, F. Shibahara, T. Maruyama, and T. Murai, "Iodine-Mediated Cyclization of N-Thioacyl-1-(2-Pyridyl)-1,2-Aminoalcohols and Their Subsequent Condensation Leading to the Formation of Novel Bis(1-Imidazo[1,5-a]pyridyl)arylmethanes," *Chemical Communications*. (2009): 7009–7011.

31. T. Murai, E. Nagaya, F. Shibabara, and T. Maruyama, "Imidazo[1,5-a] pyridine-1-Ylalkylalcohols: Synthesis via Intramolecular Cyclization of N-Thioacyl 1,2-Aminoalcohols and Their Silyl Ethers and Molecular Structures," *Organic & Biomolecular Chemistry* 10 (2012): 4943–4953.

32. B. V. Phuc, N. T. Nguyen, N. T. H. Van, et al., "Facile Iodine-Promoted Synthesis of Bis(1-Imidazo[1,5- *a*]pyridyl)arylmethanes and Exploration of Applications," *Chemical Communications* 59 (2023): 1947–1950.

33. S. Mahajan and S. D. Sawant, "C–H Functionalization of Imidazo[1,5-*a*]pyridines: A Metal-Free Approach for Methylene Insertion to Access C(sp^2)–C(sp^3)–H–C(sp^2) Bond Formation," *ACS Omega* 9 (2024): 49071–49080.

34. G. Colombo, A. Cinco, C. Vola, B. Therrien, G. A. Ardizzoia, and S. Brenna, "Blue-Emissive Fluorescent Zinc(II) Complexes with Bis(imidazo[1,5- *a*]pyridine)methane Ligands," *European Journal of Inorganic Chemistry* 27 (2024): e202400251.

35. J. Lacour, C. Ginglinger, F. Favarger, and S. Torche-Haldimann, "Application of TRISPHAT Anion as NMR Chiral Shift Reagent," *Chemical Communications* 23 (1997): 2285–2286.

36. L. Yang, D. R. Powell, and R. P. Houser, "Structural Variation in Copper(i) Complexes with Pyridylmethylamide Ligands: Structural Analysis with a New Four-Coordinate Geometry Index, τ4," *Dalton Transactions* 9 (2007): 955–964.

37. A. W. Addison, T. N. Rao, J. Reedijk, J. van Rijn, and G. C. Verschoor, "Synthesis, Structure, and Spectroscopic Properties of Copper(II) Compounds Containing Nitrogen–sulphur Donor Ligands; the Crystal and Molecular Structure of Aqua[1,7-Bis(N-Methylbenzimidazol-2′-Yl)-2,6-Dithiaheptane]copper(II) Perchlorate," *Journal of the Chemical Society, Dalton Transactions* 13 (1984): 1349–1356.

38. J.-H. Kim, S.-Y. Kim, S. Choi, H.-J. Son, and S. O. Kang, "Peripheral Ligand Effect on the Photophysical Property of Octahedral Iridium Complex: *o* -Aryl Substitution on the Phenyl Units of Homoleptic $Ir^{III}(C \hat{} C)_3$ Complexes (C ^ C = 1-Phenyl-3-Methylimidazolin-2-Ylidene-*C*, $C^{2\prime}$) for Deep Blue Phosphorescence," *Inorganic Chemistry* 60 (2021): 246–262.

39. S. Resa, A. Millán, N. Fuentes, et al., "O–H and (CO)N–H Bond Weakening by Coordination to Fe(Ii)," *Dalton Transactions* 48 (2019): 2179–2189.

40. O. V. Dolomanov, L. J. Bourhis, R. J. Gildea, J. A. K. Howard, and H. Puschmann, "*OLEX2* : A Complete Structure Solution, Refinement and Analysis Program," *Journal of Applied Crystallography* 42 (2009): 339–341.

41. C. F. Macrae, I. Sovago, S. J. Cottrell, et al., "*Mercury 4.0*: From Visualization to Analysis, Design and Prediction," *Journal of Applied Crystallography* 53 (2020): 226–235.

42. G. te Velde, F. M. Bickelhaupt, E. J. Baerends, et al., "Chemistry with ADF," *Journal of Computational Chemistry* 22 (2001): 931–967.

43. C. F. Guerra, J. G. Snijders, G. te Velde, and E. J. Baerends, "Towards an Order-N DFT Method," *Theoretical Chemistry Accounts* 99 (1998): 391–403.

44. E. J. Baerends, T. Ziegler, J. Autschbach, et al., *ADF2014, SCM, Theoretical Chemistry* (Vrije Universiteit, 2014), http://www.scm.com.

45. C. Adamo, G. E. Scuseria, and V. Barone, "Accurate Excitation Energies From Time-Dependent Density Functional Theory: Assessing the PBE0 Model," *The Journal of Chemical Physics* 111 (1999): 2889–2899.

46. A. Klamt and G. J. Schürmann, "COSMO: A New Approach to Dielectric Screening in Solvents with Explicit Expressions for the Screening Energy and its Gradient," *Journal of the Chemical Society, Perkin Transactions 2* 22 (1993): 799–805.

47. A. Klamt and V. Jonas, "Treatment of the Outlying Charge in Continuum Solvation Models," *The Journal of Chemical Physics* 105 (1996): 9972–9981.

48. C. C. Pye and T. Ziegler, "An Implementation of the Conductor-Like Screening Model of Solvation Within the Amsterdam Density Functional Package," *Theoretical Chemistry Accounts* 101 (1999): 396–408.

Supporting Information

Additional supporting information can be found online in the Supporting Information section.